Observation of carbon impurity flow in the edge stochastic magnetic field layer of Large Helical Device and its impact on the edge impurity control

Observation of Carbon Impurity Flow in the Edge Stochastic Magnetic Field Layer of Large Helical Device and its Impact on the Edge Impurity Control

T. Oishi[1,2], S. Morita[1,2], S. Y. Dai[3], M. Kobayashi[1,2], G. Kawamura[1], X. L. Huang[1], H. M. Zhang[2], Y. Liu[2], M. Goto[1,2] and the LHD Experiment Group[1]

[1] National Institute for Fusion Science, National Institutes of Natural Sciences, 322-6, Oroshi-cho, Toki, 509-5292, Japan

[2] Department of Fusion Science, Graduate University for Advanced Studies, 322-6, Oroshi-cho, Toki, 509-5292, Japan

[3] Key Laboratory of Materials Modification by Laser, Ion and Electron Beams (Ministry of Education), School of Physics, Dalian University of Technology, Dalian 116024, PR China

E-mail contact of main author: oishi@LHD.nifs.ac.jp

Abstract. The parallel flow of carbon impurity in a thick stochastic magnetic field layer called "ergodic layer" located at the edge plasma of Large Helical Device (LHD) is studied by space-resolved vacuum ultraviolet (VUV) spectroscopy using a 3 m normal incidence spectrometer. A full vertical profile of C^{3+} impurity flow is evaluated from Doppler shift of the second order of CIV line emission (2×1548.20 Å) at a horizontally-elongated plasma position of LHD. The carbon flow at the top and bottom upstream position in the ergodic layer has the same direction toward outboard side along the major radius direction. The observed flow quantitatively agrees with simulation result calculated with a three-dimensional simulation code, EMC3-EIRENE. It experimentally verifies the validity of edge parallel flow driving the impurity screening.

Keywords: impurity transport, stochastic magnetic field, VUV spectroscopy, impurity flow, helical devices

1. Introduction

Stochastization of edge magnetic fields is extensively studied not only for the ELM mitigation but also for the plasma detachment and the impurity transport [1-3]. An impurity transport phenomena, so called "impurity screening" has been attracted attention, in which the edge stochastic magnetic fields prevent impurity ions from penetrating into the core plasmas and the impurity ions are screened out toward the plasma facing materials. The first experiment of the impurity screening was conducted in Tore Supra tokamak with applying the ergodic divertor [4-6]. A theoretical model for the impurity screening has been also proposed in the viewpoint of the momentum balance of the impurity ions along the magnetic fields [7,8]. Studies on the edge stochastic magnetic field in the helical systems also have been intensively conducted. A thick stochastic magnetic field layer called "ergodic layer" of the large helical device (LHD) consists of stochastic magnetic fields with three-dimensional structure intrinsically formed by helical coils, while well-defined magnetic surfaces exist inside the last closed flux surface [9]. It is therefore extremely important to study the impurity behaviour and transport in the ergodic layer and to compare with those in the scrape-off layer of tokamaks. The effect of impurity screening has also been compared between the scrape-off layer of a tokamak and the ergodic layer of a helical device [10]. An impurity transport simulation based on a three-dimensional simulation code, EMC3-EIRENE [11,12], has been applied to the ergodic layer of LHD [13]. In the simulation, a transport model considering the parallel momentum balance on impurity ions along a magnetic field line connecting the core plasma and the divertor plate has been proposed based on the following equation;

$$m_Z \frac{\partial V_{Z/\!/}}{\partial t} = -\frac{1}{n_Z}\frac{\partial T_Z n_Z}{\partial s} + ZeE_{/\!/} + m_Z \frac{V_{i/\!/} - V_{Z/\!/}^{imp}}{\tau_s} + 0.71Z^2 \frac{\partial T_e}{\partial s} + 2.6Z^2 \frac{\partial T_i}{\partial s}, \qquad (1)$$

where the five terms at the right-hand side are contributions of impurity ion pressure gradient, parallel electric field, friction force between bulk ions and impurity ions, electron thermal force, and ion thermal force, in the order. The impurity transport which is perpendicular to the magnetic field lines is also important, therefore, the perpendicular transport is modelled by defining a perpendicular impurity diffusivity. The effect of the perpendicular diffusivity was studied and a reasonable parameter range for the diffusivity was found in [14]. In this paper, discussion is focused on the parallel transport. Among the terms in the right-hand side of Eq. (1), the friction force terms and the ion thermal force term are the dominant terms. When the ion density gradient increases, the friction force increase resulting in an impurity flow directed towards the divertor plates, which means the impurity screening. On the other hand, when the ion temperature gradient increases, the ion thermal force increases resulting in an impurity flow directed towards the core plasma, which means the impurity accumulation. In LHD, it is found that carbon impurities are screened by the presence of the ergodic layer [15] and iron impurities are more effectively screened. Effective screening for iron can be explained by the parallel transport with

following reasons; the first ionization energy of iron is lower than that of carbon as well as the velocity of iron ions is slower than that of carbon. Therefore, iron is ionized at the outer region of the ergodic layer where the friction force is more dominant due to the lower temperature, which results in the more effective screening for iron. As a result, the iron density in core plasmas of LHD is found to be extremely low despite the stainless steel vacuum vessel [16].

The precise measurement of impurity behavior is very important to develop a deeper understanding of the impurity transport in the edge ergodic layer. However, the impurity flow in the ergodic layer has not been yet measured experimentally even though it is considered to be a key mechanism to determine impurity distributions. Therefore, a profile measurement of the impurity flow is truly required to examine the validity of the theoretical modelling on the impurity transport in stochastic magnetic field layer.

This paper mainly describes impurity flow measurement based on a vacuum ultraviolet (VUV) spectroscopy technique in LHD for the contribution to the impurity transport study in edge stochastic magnetic field layer. In section 2, impurity screening in LHD characterized by carbon line emissions is briefly introduced. In section 3, the space-resolved VUV spectrometer system is explained with the measurement results of emission intensity, ion temperature and flow velocity of the carbon impurity. In section 4, interpretation of a physical meaning of the measured flow profile is discussed assisted by an impurity transport simulation based on a three-dimensional simulation code, EMC3-EIRENE. The paper is summarized in section 5.

2. Impurity screening evaluated by carbon line emissions in LHD

The LHD coil system consists of a set of two continuous superconducting helical coils with poloidal pitch number of 2 and toroidal pitch number of 10 and three pairs of superconducting poloidal coils. Figure 1 shows schematic drawings of toroidal plasma with helical coils and horizontally-elongated poloidal cross section of LHD. Poincare plot of stochastic magnetic fields in the ergodic layer under vacuum condition are shown for poloidal cross sections at horizontally-elongated plasma position of LHD for different magnetic axis configurations of R_{ax} =3.6 m and 3.9 m. The stochastic magnetic fields in the edge ergodic layer are plotted with color scale indicating the magnetic field connection length in addition to the magnetic surfaces. The ergodic layer mainly consists of stochastic magnetic field lines with connection lengths from 10 to 2000 m, which correspond to 0.5 - 100 toroidal turns in the LHD. Radial thickness of the ergodic layer varies toroidally and poloidally. When the magnetic axis is shifted outwardly, the ergodic layer is wider and the plasma size within the LCFS is smaller.

In order to evaluate the impurity screening effect due to the existence of the ergodic layer, impurity spectroscopy had been widely employed [15]. Figure 2 shows a typical waveform of a discharge with a magnetic configuration with R_{ax} = 3.6 m and B_t = 2.75 T. ECH and n-NBI power, central electron temperature and central electron density are shown together. The averaged electron density n_e was

scanned from 0.8 to 6.1×10^{13} cm^{-3}.　Intensities of carbon line emissions are monitored as an indicator of the impurity screening.　CIII (977.03 Å, 2s^2-2s2p) and CIV (1548.02 Å, 2s-2p) is measured using a 20 cm normal incidence VUV spectrometer [17] while CV (40.27 Å, 1s^2-1s2p) and CVI (33.73 Å, 1s-2p) is measured using a grazing incidence EUV spectrometer [18].　The ionization potential, E_i, for C^{2+}, C^{3+}, C^{4+}, and C^{5+} is 48 eV, 65 eV, 392 eV, and 490 eV, respectively.　Therefore, CIII and CIV radiation is emitted by carbon ions with low E_i located at the outer region of the ergodic layer, while CV and CVI radiation is emitted by carbon ions with high E_i located at inner region of the ergodic layer.

Figure 3 shows the electron density dependence of line intensity of (a) CIII, (b) CIV, (c) CV, and (d) CVI normalized by the line-averaged electron density and (e) a line ratio of (CV + CVI) / (CIII + CIV) as an indicator of the impurity screening effect.　Smaller value of the ratio means enhancement of the impurity screening effect.　The line ratio decreases with the electron density because carbon lines emitted from outer region of the ergodic layer (CIII, CIV) increase while those from inner region (CV, CVI) decrease. It indicates enhancement of the impurity screening in high density regime.　Figure 3(e) also shows a comparison of the line ratio between the inward-shifted magnetic configuration with R_{ax} = 3.6 m and the outward-shifted magnetic configurations with R_{ax} = 3.9 m.　The impurity screening effect is more obvious in the outward-shifted configuration.　It has been known that the edge density profile is flat in the outward-shifted magnetic configuration for the same line-averaged electron density.　Therefore, the friction force becomes dominant in the thick ergodic layer, which results in the more effective impurity screening [15].

3.　Measurements of emission intensity, ion temperature and flow velocity of the carbon impurity

Space-resolved vacuum ultraviolet (VUV) spectroscopy using a 3 m normal incidence spectrometer is utilized to measure impurity emission profile in the edge and divertor plasmas of LHD in wavelength range of 300 - 3200 Å [19].　A 3m normal incidence VUV spectrometer (McPherson model 2253) is installed on an outboard midplane diagnostic port as shown in Fig. 4.　A back-illuminated CCD detector (Andor model DO934-BN: 1024 × 1024 pixels) is placed at the position of the exit slit of the spectrometer for measuring a focal image of VUV line emissions.　A high wavelength dispersion of 0.037 Å/pixel enables Doppler profile measurement of the impurity lines basically over the whole wavelength range [20].　The viewing angle can be switched between "full profile measurement" mode to cover an entire vertical region of the elliptical LHD plasma at horizontally-elongated poloidal plasma cross section to measure the top-to-bottom vertical profile and "edge profile measurement" to focus the viewing angle on the bottom edge with a high spatial resolution for observations of vertical impurity profile in the ergodic layer as shown in Fig. 4.

The CCD signals are summed up every 10 vertical pixels and replaced into single vertical channel.　The CCD image with 1024 × 1024 pixels is then changed into that with 102 × 1024 channels.　The observable region is resolved by 102 observation chords.　Each profile image is taken with a time interval of 200 ms. Figure 5 shows spectra of the second order of CIV line emission (2 × 1548.20 Å) at different vertical

positions of (a) Z = 479 mm at the top edge of the ergodic layer, (b) Z = 5 mm which is close to the midplane, and (c) Z = -486 mm at the bottom edge of the ergodic layer for inward-shifted magnetic configuration with R_{ax} = 3.6 m.   The discharge conditions are the same as those in Fig. 2.   Spectral data in the steady state phase shown in Fig. 5 were averaged over from 4.0 to 5.0 s in the discharge shown in Fig. 2.   Signal intensities in the figure are normalized to be unity for simplicity.   We successfully observed the Doppler-shift which corresponds to the flow of C^{3+} ions in observation chords located at both the top and bottom edges of the ergodic layer as shown in Figs. 5 (a) and (c).   The flow velocity along the sightline, v, is given by $v = c (\Delta\lambda / \lambda)$, where c is the light speed, $\Delta\lambda$ the Doppler-shift and λ the wavelength of line emission.   At present, a spectral peak of the CIV spectrum in a recombination phase at the plasma termination, as shown in the hatched region in the discharge waveform from 5.4 to 5.6 s in Fig. 2, is regarded as the reference of the Doppler shift because the plasma temperature is extremely low and any plasma flow seems to have already disappeared.

Figure 6 (a) shows the full vertical profiles of (a) CIV line intensity, (b) ion temperature, and (c) flow velocity derived from the Doppler profile of CIV line with the wavelength of 1548.20 × 2 Å for $n_e = 6.0 \times 10^{13}$ cm^{-3} and R_{ax} = 3.6 m.   The error bars of the values shown in Fig. 6 (a-c) are determined from the fitting error by the Gaussian profile.   The observation range of the VUV spectroscopy are illustrated in Fig. 6(d).   Two solid arrows in Fig. 6 (c) correspond to the observation chords located with two solid arrows in Fig. 6 (d).   It is known that the spatial profile of the CIV intensity has a steep peak in the ergodic layer [21].   CIV emission is released only in the outermost region of the ergodic layer in LHD plasmas because the low ionization energy of 65 eV for C^{3+} ions causes less fractional abundance in the core plasma.   Therefore, the peak of the intensity profile outside the LCFS shown in Fig. 6 (a) is a result of line integration in a long path along the sightline through the ergodic layer at the bottom and top edge of the holizontally-elongated elliptical plasma.   The intensity peak around Z = 0 mm in Fig. 6 (a) is superposition of emissions from inboard and outboard divertor trajectories.   Emission peaks from the top and bottom edges have an asymmetry depending on the direction of the toroidal magnetic field.   In the present study, the bottom peak has a larger intensity so that that it appears clearer than the top peak [22]. The T_i profile also indicates the edge T_i in the ergodic layer at corresponding vertical position.   Figure 6(c) shows a flow profile of C^{3+} impurity.   The measured flow velocity in Fig. 6(c) is projection of the flow along the observation chord which can approximately be considered to be the direction of the plasma major radius.   Therefore, a variable of v_R is used to indicate the measured flow value.   Positive and negative sign in the horizontal axis of Fig. 6(c) corresponds to the outboard and inboard direction along the plasma major radius, respectively.   From the figure it is found that the flow direction is the same, i.e. the outboard direction, for both the top (Z = 480 mm) and bottom (Z = -480 mm) edges of the ergodic layer.   A synthetic profile of the C^{3+} flow calculated with the impurity transport simulation based on a three-dimensional simulation code, EMC3-EIRENE is also plotted with solid line in Fig. 6(c).   To obtain a synthetic vertical profile of the flow, v_R, local value of the calculated flow projected in the major radius direction, $v_{R,loc}$, is line-integrated weighted by emission intensity along each observation chord as follows,

$$\int v_{R,loc}\, \varepsilon\, n_{C^{3+}} n_e\, dl \,/\, \int \varepsilon\, n_{C^{3+}} n_e\, dl, \qquad (2)$$

where ε is an emission coeficcient of the CIV line, n_c^{3+} is density of C^{3+} ion, and n_e is electron density. The experiment and the simulation exhibit an excellent agreement with each other. The simulation code employs an impurity transport model that the impurity flow is driven by a momentum balance on the impurity ions along the magnetic field line. The friction force term is much larger than the ion thermal force term in the momentum balance in the present case, which will be discussed later in the next section. Figure 7 shows the flow at the top and bottom edges of the ergodic layer as a function of density. It indicates that the flow which has the same direction as the friction force increases with the density. The result supports a prediction by the simulation that the friction force becomes more dominant in the force balance in higher density regime, which results in the increase of impurity flow causing the impurity screening.

The edge flow profile is investigated with high spatial resolution by using the viewing angle of the edge profile measurement of the VUV spectroscopy. Figure 8 shows vertical profiles at the bottom edge of the ergodic layer of (a) CIV line intensity, (b) ion temperature, and (c) flow velocity derived from CIV 1548.20 $\times$ 2 Å line emission measured by VUV spectroscopy for n_e = 2.9, 4.2, and 6.0×10^{13} cm^{-3} with a magnetic configuration with R_{ax} = 3.6 m and B_t = 2.75 T. The observation range of the edge profile measurement of the VUV spectroscopy is also shown in Fig. 8(d). As increasing the electron density, the flow velocity toward the outboard direction develops clearly with the maximum value at Z = -480 mm. We compared the results with a magnetic configuration of R_{ax} = 3.9 m and B_t = 2.539 T as shown in Fig. 9. Figure 9(c) indicates that the flow is directed toward the inboard direction with the maximum value at Z = -480 mm. This direction is also same as the friction force in the parallel momentum balance for R_{ax} = 3.9 m calculated with EMC3-EIRENE code which will be described later, even though it is opposite direction to that of R_{ax} = 3.6 m case. The maximum values of the flow did not depend on the electron density within the density range employed in this experiment.

4. Comparison of the impurity flow between experiment and simulation

The carbon flow measured with spectroscopic method is compared with the impurity transport simulation based on the EMC3-EIRENE code for the first time. The simulation is carried out with the electron density at the last closed flux surface (LCFS), $n_{e,\ LCFS}$, of 6.0×10^{13} cm^{-3} and the auxiliary heating power, P_{in}, of 10 MW, which is the same discharge condition as the result in Fig. 6. Figure 10 shows a colour contour of the simulation result for the flow component of C^{3+} impurity flow parallel to magnetic field lines projected to the major radius direction. The yellow and blue colour means that the flow has a major radius component in outboard and inboard direction, respectively. The magnetic field lines at the top and bottom edges of the ergodic layer are illustrated by the black solid arrows as B_{top} and B_{bottom}, respectively. The green thick dashed arrows indicate the flow velocity and direction parallel to the magnetic field line, $V_{//}$, at the top and bottom edges. In this calculation result, the absolute value of $V_{//}$ is about 50 km/s

both at the top and bottom edges. It should be noted here that the toroidal component of $V_{//}$ has an opposite direction between the top and bottom edges, while the major radius component of $V_{//}$ has the same direction toward outboard side. The detailed studies of impurity flow direction are presented in the accompanying paper [23]. A synthetic profile of the simulated flow is also shown in Fig. 6(c) with solid line, which is obtained by integrating the Doppler-shifted CIV intensities along the observation chord. The excellent agreement between experiment and simulation in the present study concludes that the parallel flow in the ergodic layer can be well explained by the presently used theoretical modelling on the edge impurity transport. Therefore, the impurity parallel flow can be mainly determined by the momentum balance along the magnetic field line. In particular, the friction force between impurity and bulk ions and the ion thermal force driven by the ion temperature gradient are dominant terms in the momentum balance. The calculated friction force, which is expressed as the third term of the right-hand side of Eq. (1), has the maximum value at both the top and bottom edges of the ergodic layer where the impurity parallel flow also takes the maximum value. The impurity screening driven by the friction force can be more effective at higher electron density range. The density dependence of the flow in the modelling can be also clarified by the experimental result shown in Fig. 7 and Fig. 8(c).

On the other hand, Fig. 11 shows the simulation results for another magnetic configurations of R_{ax} = 3.9 m and B_t = 2.539 T for 4.0 $\times$ 10^{13} cm^{-3} and P_{in} of 10 MW. When the magnetic axis is shifted outwardly, the ergodic layer is wider and the plasma size within LCFS is smaller. It should be noted that the toroidal component of $V_{//}$ has an opposite direction between the top and bottom edges here again, while the major radius component of $V_{//}$ has the same direction, namely, the direction toward inboard side for outward-shifted configuration with R_{ax} = 3.9 m while the direction toward outboard side for inward-shifted configuration with R_{ax} = 3.6 m. It agrees with the experimentally observed flow direction toward inborad direction as shown in Fig. 9(c) for R_{ax} = 3.9 m. The agreement concludes that the parallel flow in the ergodic layer can be well explained by the presently used theoretical modelling on the edge impurity transport.

Finally, the electron density dependence of the maximum value of measured flow is summarized in Fig. 12. Now we understand that all plots in the figure have directions same as the friction force even though the flow directions are opposite between R_{ax} = 3.6 m and R_{ax} = 3.9 m. In the case of R_{ax} = 3.9 m, the flow has a large value even in the low density regime. The reason why flow velocity is almost constant with electron density for Rax = 3.9 m has not been clarified yet. It might have some relationship with the fact that the impurity screening effect for R_{ax} = 3.9 m is larger than R_{ax} = 3.6 m. It has been known that the edge density profile is flat in the outward-shifted magnetic configuration for the same line-averaged electron density. Therefore, the friction force becomes dominant in the thick ergodic layer, which results in the more effective impurity screening. Further simulations in the low density regime are needed to clarify the density dependence of the impurity flow, which remains as a future study.

5. Summary

The parallel flow of carbon impurity in a thick stochastic magnetic field layer called "ergodic layer" located at the edge plasma of Large Helical Device (LHD) is studied by space-resolved VUV spectroscopy using a 3 m normal incidence spectrometer.   A full vertical profile of C^{3+} impurity flow is evaluated from Doppler shift of the second order of CIV line emission (2×1548.20 Å) at a horizontally-elongated plasma position of LHD for a hydrogen discharge with $R_{ax} = 3.6$ m, $B_t = 2.75$ T, $n_e = 6.0 \times 10^{13}$ cm^{-3} and $P_{in} = 10$ MW.   It is found that the the carbon flow at the top and bottom edges in the ergodic layer has the same direction toward outboard side along the major radius direction.   The flow velocity increases with the density at both the top and bottom edges of the ergodic layer.

The simulation result of C^{3+} impurity flow parallel to the magnetic field lines calculated with a three-dimensional simulation code, EMC3-EIRENE indicates that the major radius component of the flow has the same direction toward outboard side at the top and bottom edges in the ergodic layer.   The experiment and the simulation agree with each other quantitatively, which concludes that the parallel flow in the ergodic layer can be well explained by the presently used theoretical modelling.   In particular, the impurity screening driven by the friction force between impurity and bulk ions can be more effective at higher electron density range.   The density dependence of the flow in the modelling can be also clarified by the experimental result.

References

[1]   P. C. Stangeby and G. M. McCracken, "Plasma boundary phenomena in tokamaks," Nucl. Fusion **30** (1990) 1225.

[2]   T. E. Evans, R. A. Moyer, P. R. Thomas *et al.*, "Suppression of Large Edge-Localized Modes in High-Confinement DIII-D Plasmas with a Stochastic Magnetic Boundary," Phys. Rev. Lett. **92** (2004) 235003.

[3]   M. Kobayashi, S. Masuzaki, I. Yamada *et al.*, "Detachment stabilization with n/m=1/1 resonant magnetic perturbation field applied to the stochastic magnetic boundary of the Large Helical Device," Phys. Plasmas **17** (2010) 056111.

[4]   C. Breton, C. De Michelis, M. Mattioli *et al.*, "Plasma decontamination during preliminary ergodic divertor experiments in TORE SUPRA," Nucl. Fusion **31** (1991) 1774.

[5]   Ph. Ghendrih, H. Capes, C. DeMichelis *et al.*, "A review of experiments and theory on stochastic scrape-off-layers," Plasma Phys. Control. Fusion **34** (1992) 2007.

[6]   C. De Michelis, A. Grosman, X. Garbet *et al.*, "Characteristics of ergodic divertor plasmas in the Tore Supra tokamak," Nucl. Fusion **35** (1995) 1133.

[7]   M. Z. Tokar, H. Lasaar, W. Mandl *et al.*, "Modelling of plasma and impurity behaviour in a tokamak with a stochastic layer," Plasma Phys. Control. Fusion **39** (1997) 569.

[8]   M. Z. Tokar, "On transport, in particular of impurities, in a stochastic magnetic field," Phys. Plasmas **7** (1999) 2808.

[9]   T. Morisaki, K. Narihara, S. Masuzaki *et al.*, "Ergodic edge region of large helical device," J. Nucl. Mater. **313-316** (2003) 548.

[10]   M. Kobayashi, S. Morita, C. F. Dong *et al.*, "Edge impurity transport study in the stochastic layer of LHD and the scrape-off layer of HL-2A," Nucl. Fusion **53** (2013) 033011.

[11]   Y. Feng, F. Sardei, J. Kisslinger *et al.*, "3D Edge Modeling and Island Divertor Physics," Contrib. Plasma Phys. **44** (2004) 57.

[12]   D. Reiter, M. Baelmans and P. Börner, "The EIRENE and B2-EIRENE Codes," Fusion Sci. Technol. **47** (2005) 172.

[13]   M. Kobayashi, Y. Feng, S. Morita *et al.*, "Model prediction of impurity retention in stochastic magnetic boundary and comparison with edge carbon emission in LHD", J. Nucl. Mater. **390-391** (2009) 325.

[14]   S. Y. Dai, M. Kobayashi, G. Kawamura *et al.*, "EMC3-EIRENE modelling of edge impurity transport in the stochastic layer of the large helical device compared with extreme ultraviolet emission measurements," Nucl. Fusion **56** (2016) 066005.

[15]   M. B. Chowdhuri, S. Morita, M. Kobayashi *et al.*, "Experimental study of impurity screening in the edge ergodic layer of the Large Helical Device using carbon emissions of CIII to CVI," Phys. Plasmas **16** (2009) 062502.

[16]   S. Morita, C. F. Dong, M. Kobayashi *et al.*, "Effective screening of iron impurities in the ergodic layer of the Large Helical Device with a metallic first wall," Nucl. Fusion **53** (2013) 093017.

[17]   T. Oishi, S. Morita, X. L. Huang *et al.*, "Line Spectrum of Tungsten Ions at Low Ionization Stages in Large Helical Device in Wavelength Range of 300-2400 Å Measured Using 20 cm Normal Incidence VUV Spectrometers," Plasma Fus. Res. **10** (2015) 3402031.

[18] M. B. Chowdhuri, S. Morita and M. Goto, "Characteristics of an absolutely calibrated flat-field extreme ultraviolet spectrometer in the 10–130 Å range for fusion plasma diagnostics," Appl. Opt. **47** (2008) 135.

[19] T. Oishi, S. Morita, C. F. Dong *et al.*, "Space-resolved 3 m normal incidence spectrometer for edge impurity diagnostics in the Large Helical Device,"Appl. Opt. **53** (2014) 6900.

[20] T. Oishi, S. Morita, X. L. Huang *et al.*, "Observation of W IV-W VII line emissions in wavelength range of 495-1475 Å in the large helical device," Physica Scripta **91** (2016) 025602.

[21] C. F. Dong, S. Morita, M. Kobayashi *et al.*, "A study on plasma edge boundary in ergodic layer of LHD based on radial profile measurement of impurity line emissions," Phys. Plasmas **18** (2011) 082511.

[22] T. Oishi, S. Morita, X. L. Huang *et al.*, "Effect of impurity source locations on up-down asymmetry in impurity distributions in the ergodic layer of large helical device," Nuclear Materials and Energy (2017) *in press*, DOI: 10.1016/j.nme.2017.04.002

[23] S. Y. Dai *et al.*, "First EMC3-EIRENE modelling of edge impurity flow velocity in the Large Helical Device compared with the experiment," *to be submitted to* Nucl. Fusion.
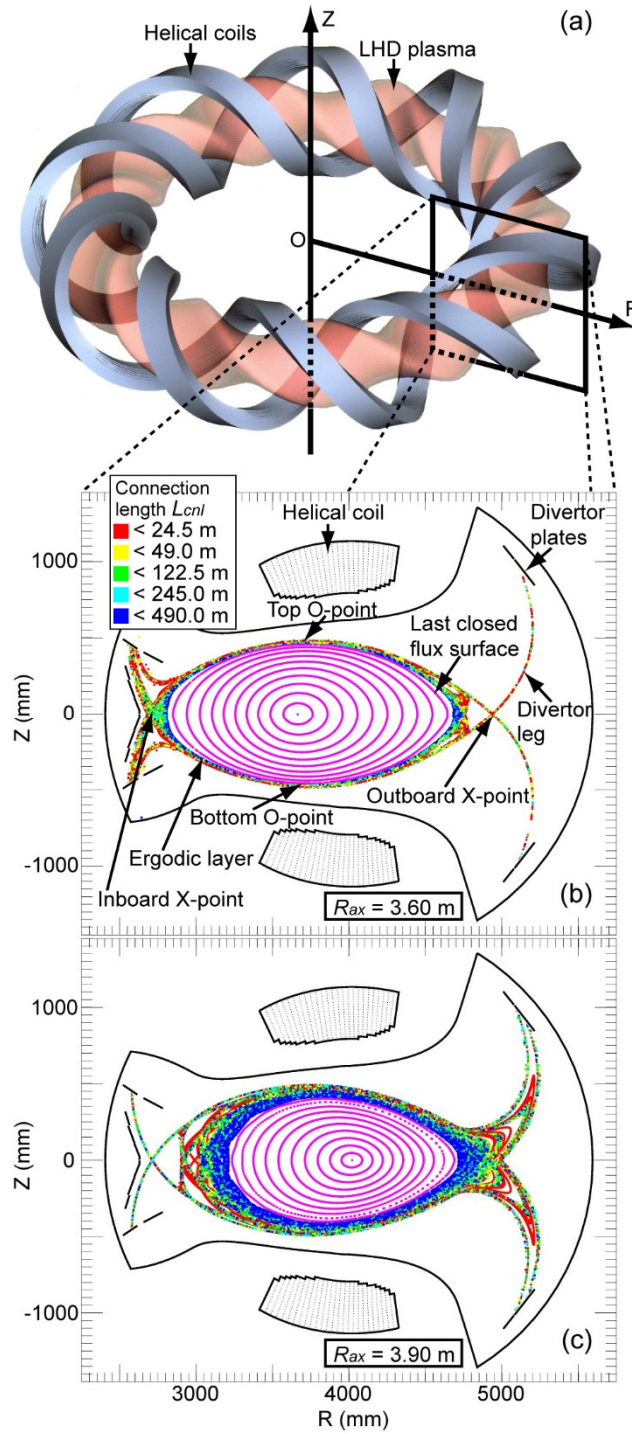
Fig. 1. (a) Schematic drawings of toroidal plasma with helical coils and horizontally-elongated poloidal cross section of LHD. Z and R mean vertical and horizontal coordinates with the torus center as the origin of the coordinate system, respectively. Poincare plot of stochastic magnetic fields at ergodic layer in vacuum condition are shown in poloidal cross sections at horizontally-elongated plasma position of LHD for different magnetic axis configurations of R_{ax} = (b) 3.6 m and (c) 3.9 m, respectively.
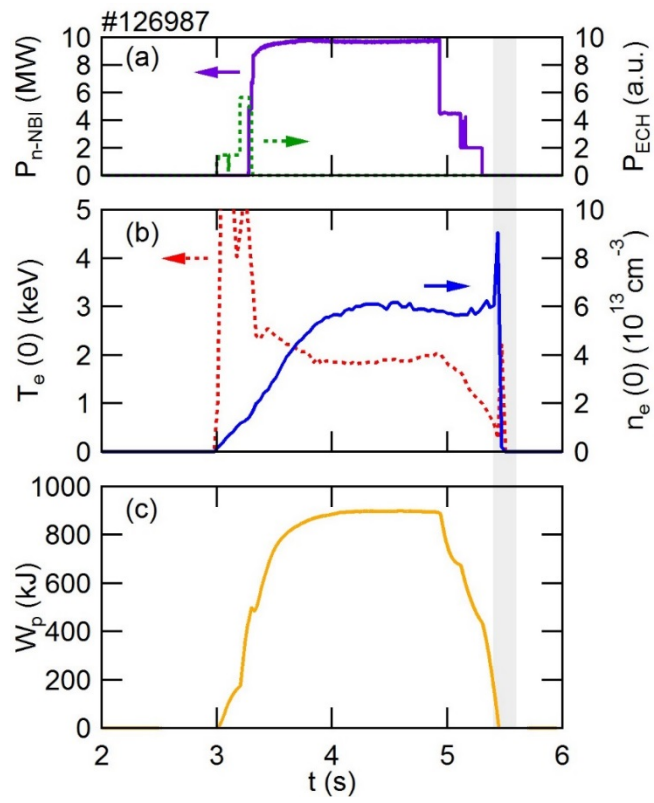
Fig. 2.   Typical waveform of a discharge in which the space-resolved VUV spectroscopy is attempted. (a) ECH and n-NBI power, (b) central electron temperature and central electron density, and (c) plasma stored energy.
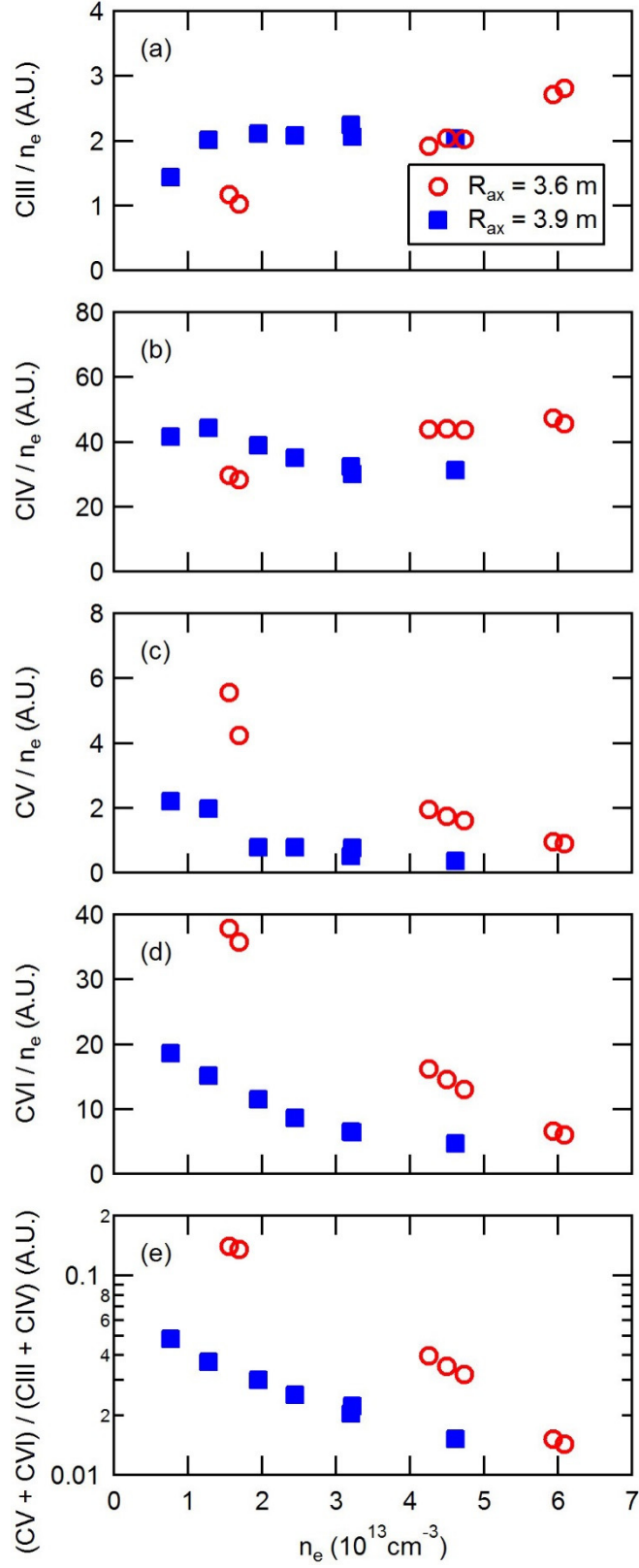
Fig. 3. Electron density dependence of line intensity of (a) CIII, (b) CIV, (c) CV, (d) CVI normalized by the electron density and (e) line ratio (CV + CVI) / (CIII + CIV) for inward-shifted magnetic configuration with R_{ax} = 3.6 m and outward-shifted magnetic configuration with R_{ax} = 3.9 m.

13
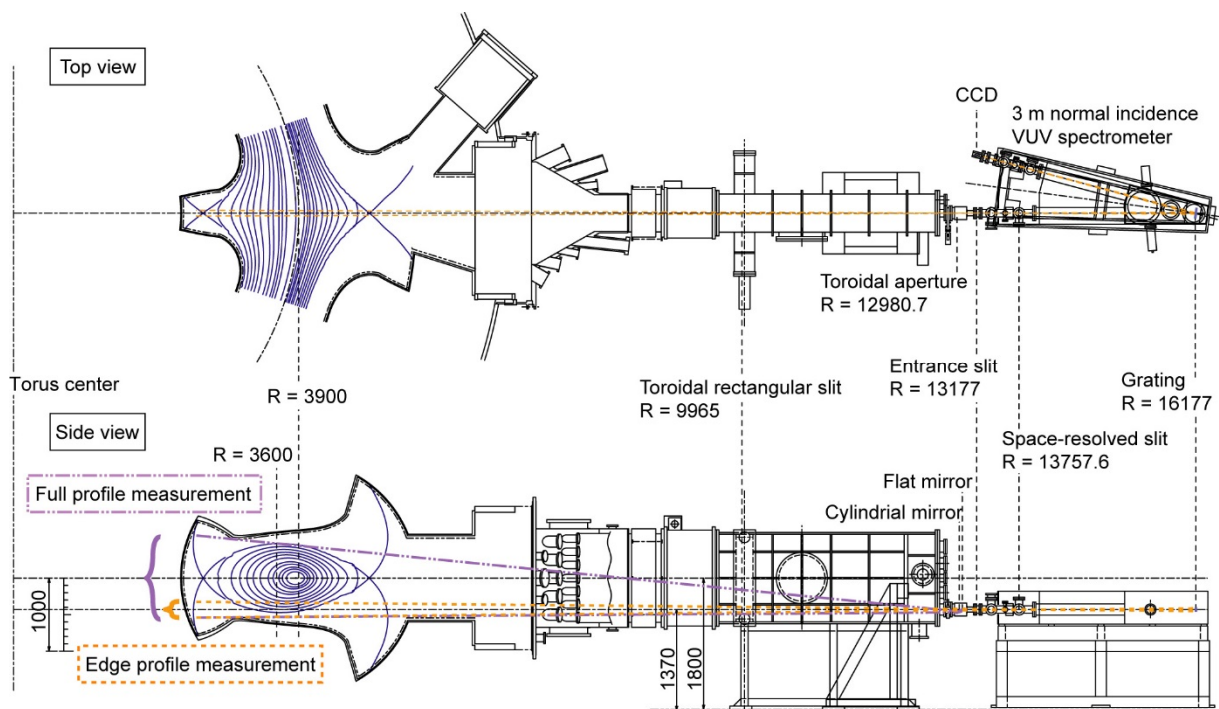
Fig. 4. Schematic drawings of space-resolved VUV spectroscopy system using 3 m normal incidence VUV spectrometer in LHD.
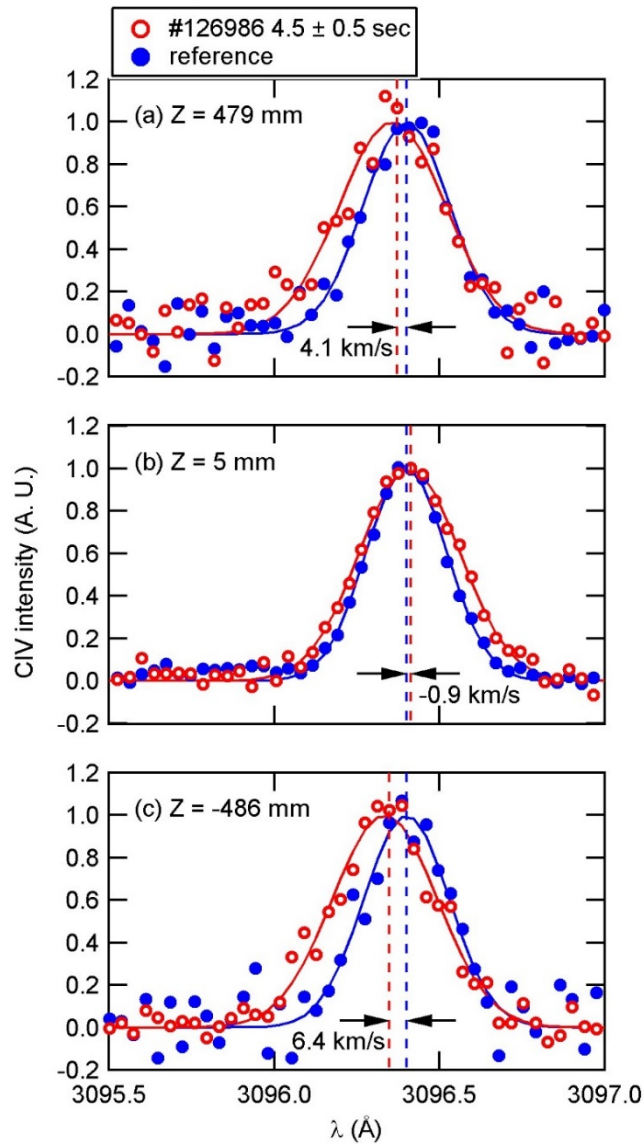
Fig. 5. Wavelength spectra of CIV 1548.20 × 2 Å at different vertical positions of (a) Z = 479 mm at the top edge of the ergodic layer, (b) Z = 5 mm close to the midplane, and (c) Z = -486 mm at the bottom edge of the ergodic layer for inward-shifted magnetic configuration with R_{ax} = 3.6 m.
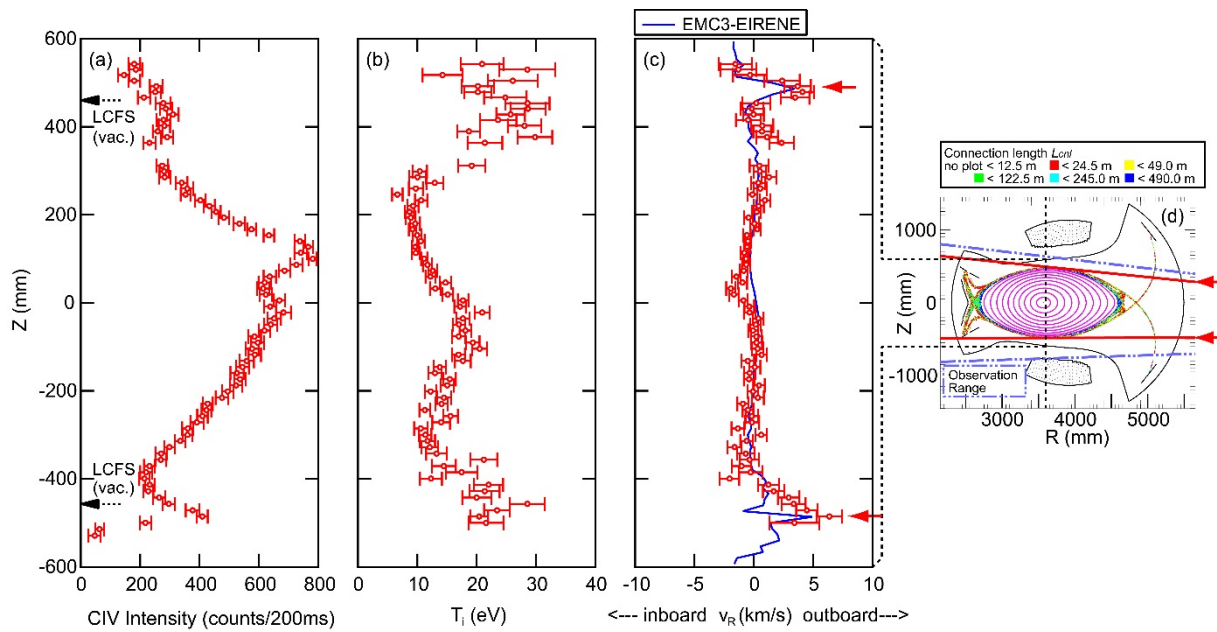
Fig. 6.   Full vertical profiles of (a) CIV line intensity, (b) ion temperature, and (c) flow velocity derived from the Doppler profile of the second order of CIV line emission (2×1548.20 Å) measured by VUV spectroscopy for inward-shifted magnetic configuration with $R_{ax} = 3.6$ m.   A synthetic profile of the C^{3+} flow simulated with EMC3-EIRENE code is also plotted with solid line in (c).   (d) The observation range of the VUV spectroscopy.   Two solid arrows in (c) correspond to the observation chords located with two solid arrows in (d).

16
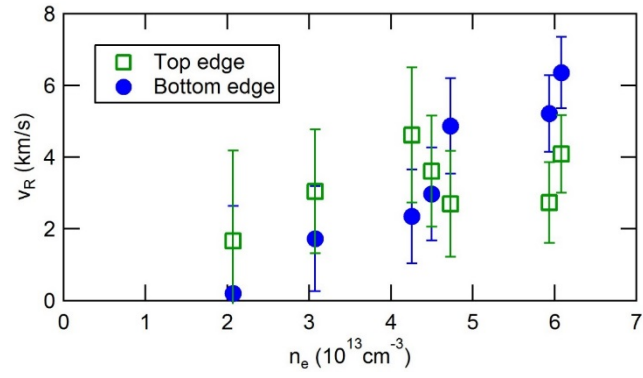
Fig. 7. Observed C^{3+} flow at the top and bottom edges of the ergodic layer as a function of the electron density for inward-shifted magnetic configuration with R_{ax} = 3.6 m.
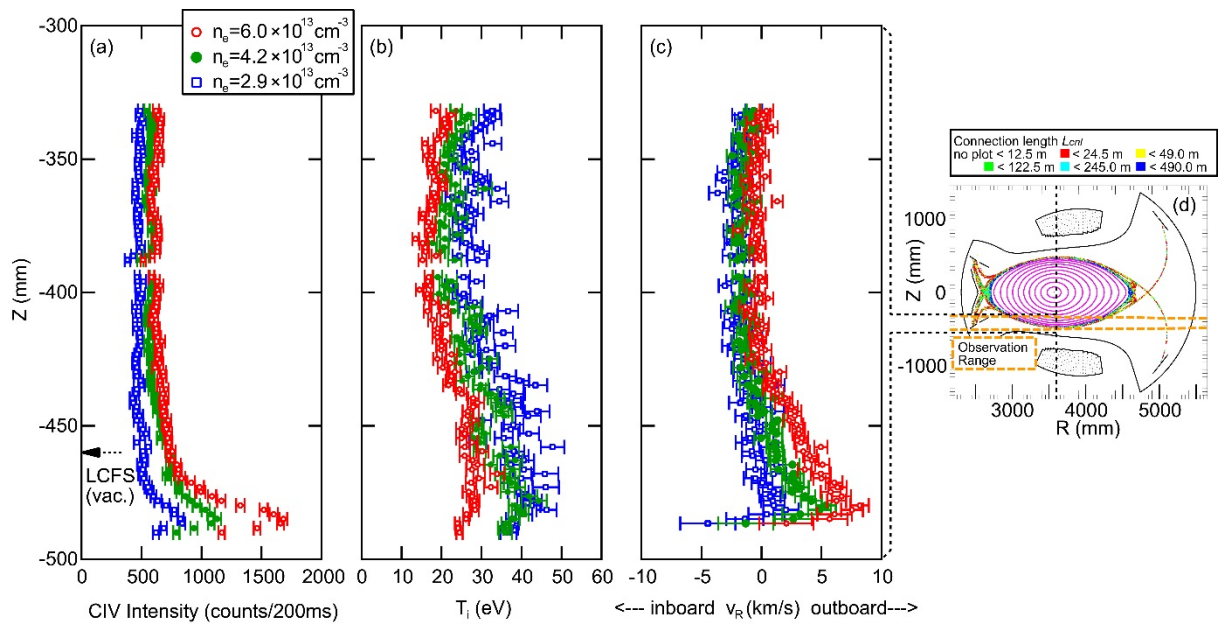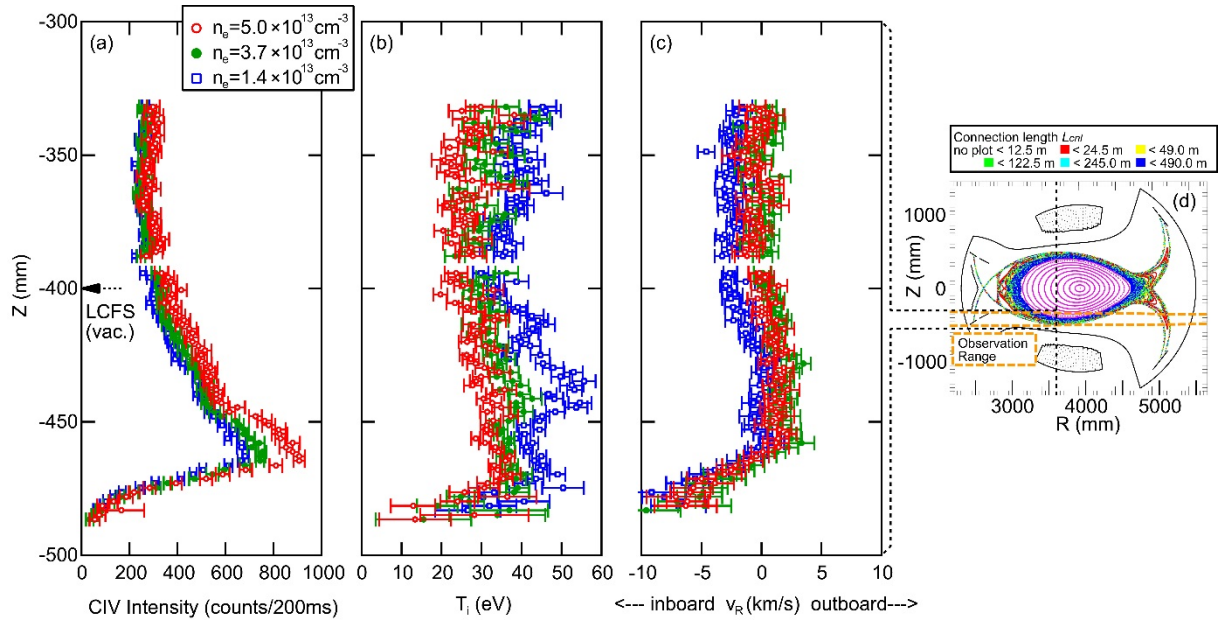
Fig. 8　Vertical profiles at the bottom edge of the ergodic layer of (a) CIV line intensity, (b) ion temperature, and (c) flow velocity derived from the Doppler profile of the second order of CIV line emission (2 × 1548.20 Å) measured by VUV spectroscopy for inward-shifted magnetic configuration with R_{ax} = 3.6 m.　(d) The observation range of the VUV spectroscopy.

18

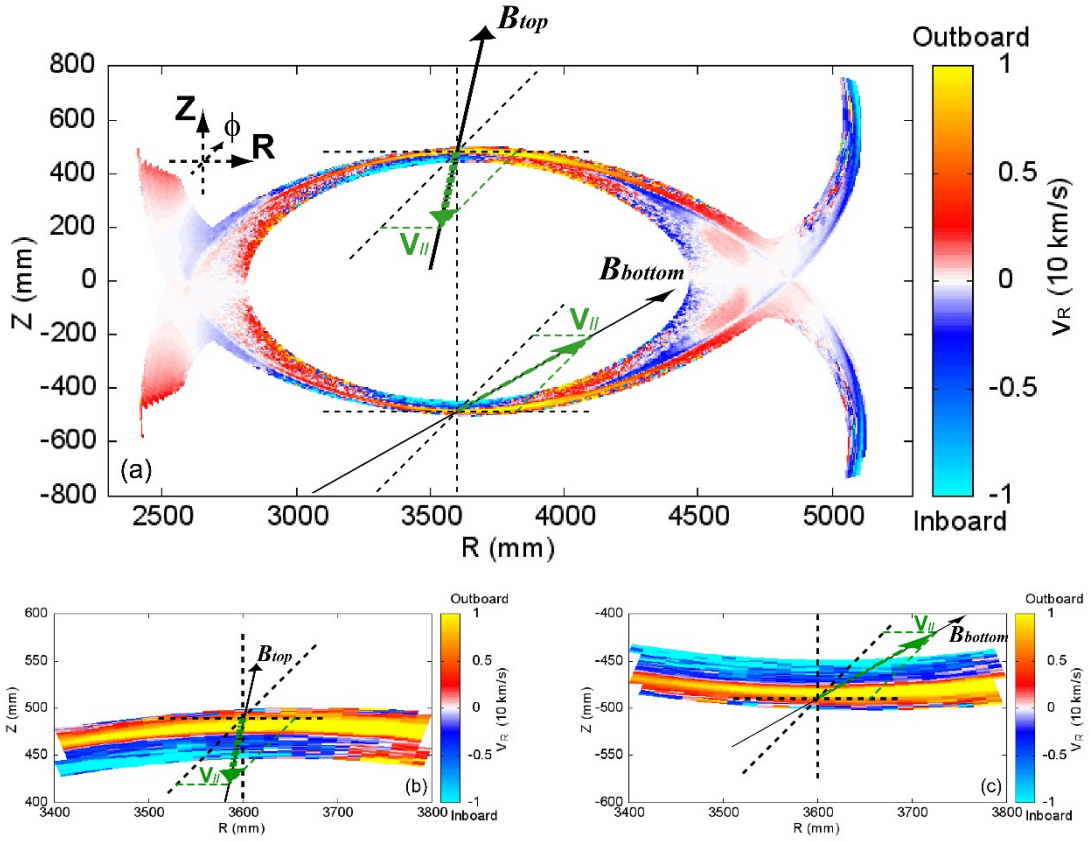Fig. 9   Vertical profiles at the bottom edge of the ergodic layer of (a) CIV line intensity, (b) ion temperature, and (c) flow velocity derived from the Doppler profile of the second order of CIV line emission (2 × 1548.20 Å) measured by VUV spectroscopy for outward-shifted magnetic configuration with R_{ax} = 3.9 m.   (d) The observation range of the VUV spectroscopy.

Fig. 10.   Flow component of C^{3+} impurity flow parallel to magnetic field lines projected to the direction of the major radius calculated with EMC3-EIRENE code for R_{ax} = 3.6 m.   Magnetic field lines at the top and bottom edges of the ergodic layer, B_{top} and B_{bottom}, and the direction of flow velocity parallel to the magnetic field line, $V_{//}$, are illustrated together in (a) holizontally-elongated poloidal cross section and enlarged views of (b) top and (c) bottom edges of the ergodic layer.
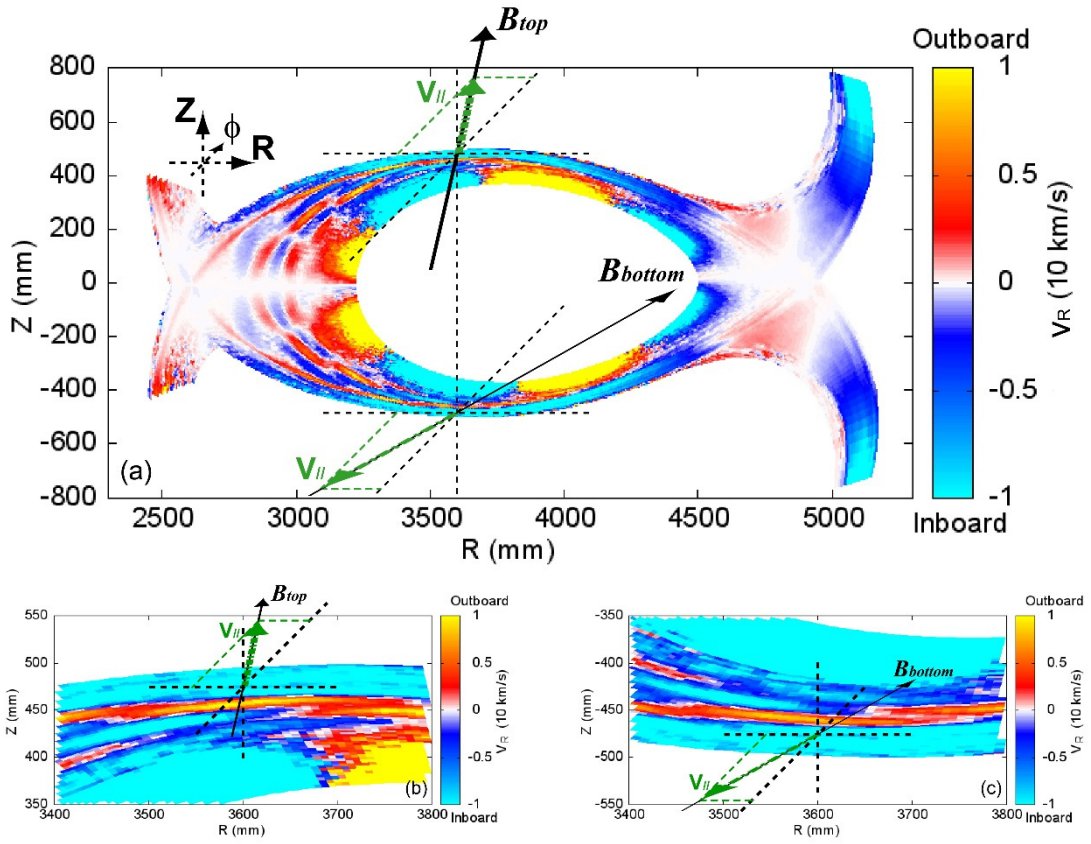
Fig. 11.   Flow component of C^{3+} impurity flow parallel to magnetic field lines projected to the direction of the major radius calculated with EMC3-EIRENE code for $R_{ax} = 3.9$ m.   Magnetic field lines at the top and bottom edges of the ergodic layer, B_{top} and B_{bottom}, and the direction of flow velocity parallel to the magnetic field line, $V_{//}$, are illustrated together in (a) holizontally-elongated poloidal cross section and enlarged views of (b) top and (c) bottom edges of the ergodic layer.
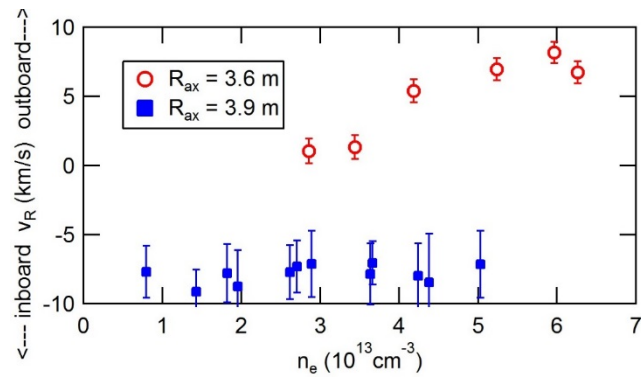
21

Fig. 12.   Observed C^{3+} flow at the bottom edge of the ergodic layer as a function of density for inward-shifted magnetic configuration with R_{ax} = 3.6 m and outward-shifted magnetic configuration with R_{ax} = 3.9 m.